Evidence of atypical structural flexibility of the active site surrounding of an [FeFe] hydrogenase from *Clostridium beijerinkii.*

Patrick S. Corrigan[1], Sean H. Majer[1], Alexey Silakov[1]*

[1] Pennsylvania State University, 104 Chemistry Building, University Park, PA, 16802, USA

*To whom correspondence should be addressed. Phone, (814) 863-7248; email aus40@psu.edu

ABSTRACT

[FeFe] hydrogenase from *Clostridium beijerinkii* (*Cb*HydA1) is an unusual hydrogenase in that it can withstand prolonged exposure to O_2 by reversibly converting into an O_2-protected, inactive state (H_{inact}). It has been indicated in the past that an atypical conformation of the "$SC_{367}CP$" loop near the $[2Fe]_H$ portion of the six-iron active site (H-cluster) allows the Cys367 residue to adopt an "off-H^+-pathway" orientation promoting a facile transition of the cofactor to H_{inact}. Here, we investigated the electronic structure of the H-cluster in the oxidized state (H_{ox}) that directly converts to H_{inact} under oxidizing conditions and the related CO-inhibited state (H_{ox}-CO). We demonstrate that both states exhibit two distinct forms in Electron Paramagnetic Resonance (EPR) spectroscopy. The ratio between the two forms is pH-dependent but also sensitive to the buffer choice. Our IR and EPR analysis illustrate that the spectral heterogeneity is due to a perturbation of the coordination environment of the H-cluster's $[4Fe4S]_H$ subcluster without affecting the $[2Fe]_H$ subcluster. Overall, we conclude that the observation of two spectral components per state is evidence of heterogeneity of the environment of the H-cluster likely associated with conformational mobility of the SCCP loop. Such flexibility may allow Cys367 to switch rapidly between off- and on-H^+-pathway rotamers. Consequently, we believe such structural mobility may be the key to maintaining high enzymatic activity while allowing a facile transition to the O_2-protected state.

INTRODUCTION

[FeFe] hydrogenases catalyze reversible heterolytic splitting of H_2.[1–4] The ability to produce hydrogen at staggering rates (~10,000 turnovers per second) makes [FeFe] hydrogenases potential candidates for biological H_2 production in engineered organisms as a carbon-neutral alternative to currently employed ways of generating H_2. [5–9] Many anaerobic organisms are replete with such enzymes that perform various metabolic functions. [4,10–13] The active site of [FeFe] hydrogenases (H-cluster) consists of a complex six-iron cluster formed by a ferredoxin-like, four-Cys coordinated $[4Fe4S]_H$ subcluster connected to a $[2Fe]_H$ subcluster via a Cys-thiolate bridge (see **figure 1**).[14–17] The $[2Fe]_H$ subcluster is a biologically unique cofactor consisting of two Fe ions coordinated by three CO and two CN^- ligands as well as an azadithiolate (*adt*= $[(SCH_2)_2NH]^{2-}$) bridge. The cysteine near the *adt* bridge is proposed to play an essential part in the conserved H^+-transfer pathway in bidirectional [FeFe] hydrogenases.[18–24] The notable divergences are the sensory [FeFe] hydrogenases missing this and other proton-transfer residues.[12,25] Apart from the active site, most [FeFe] hydrogenases contain additional metallocofactors, such as [4Fe4S] ferredoxin-like clusters.[10,11,26]

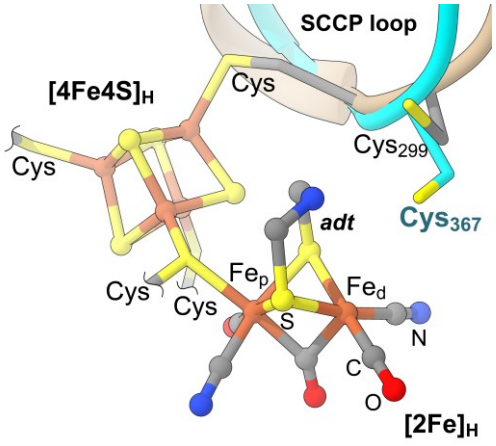

Figure 1. Structure of the H-cluster. Tan and cyan SCCP loops are from structures of *Cp*I (PDB: 4XDC) and *Cb*A5H (PDB: 6TTL), respectively, and are aligned to by the position of the H-cluster.

One of the promising concepts for bio-H_2 production is coupling an [FeFe] hydrogenase to photosystem I for light-driven H_2 generation in phototrophic bacteria or algae.[5–9] A major drawback of such an approach is that the inevitable presence of molecular oxygen (O_2) in photosynthetic organisms would cause irreversible degradation of the active center of most known [FeFe] hydrogenases. While the exact mechanism of degradation is still debated, it is accepted that the interaction of O_2 with the H-cluster leads to the formation of harmful reactive oxygen species (ROS). Intriguingly, it has been indicated that oxygen does not degrade the protein in the absence of the complete H-cluster, suggesting that O_2 must be able to react with the active H-cluster to generate ROS. [27–30]

Morra et al.[31] have shown that [FeFe] hydrogenase from *Clostridium beijerinkii* SM10 (termed *Cb*A5H) can fully reactivate after removing oxygen from the sample solution contradicting the established paradigm of O_2 sensitivity of this class of enzymes. We recently showed that a near-identical homolog from *Clostridium beijerinkii* NCIMB 14988 (*Cb*HydA1) similarly tolerates the presence of oxygen even in the absence of any oxygen scavenging agents such as sodium dithionite.[32] We confirmed that the enzyme transitions to the inactive, O_2-protected state (H_{inact}), under aerobically or chemically oxidizing conditions. Our spectroelectrochemical experiments showed that the transition to H_{inact} is thermodynamically favorable at mildly oxidizing potentials, less than 100 mV above the Nernst potential of the H^+/H_2 couple.

The unusual occurrence of a hydride-bound state (H_{hyd}) at low potentials and neutral pH led us to suggest a natural disruption of the H^+-transfer pathway in *Cb*HydA1.[32] We hypothesized that the cause of the disruption is the reorientation of Cys367 to a non-productive rotamer. Taking the sulfide-bound H_{inact} (hereafter called H_{inact}-SH) in [FeFe] hydrogenase from *Desulfovibrio desulfuricans* (*Dd*HydAB) as a precedent,[14] we then suggested that the H_{inact} state in *Cb*HydA1 has an Fe-S bond between the distal Fe of the $[2Fe]_H$ subcluster (Fe_d) and the Cys367 sidechain. Theoretical calculations of the vibration frequencies of CN^- and CO ligands of the H_{inact} state modeled with a Cys367 bound to the H-cluster agree reasonably well with our experimental observations. However, according to our calculations, another plausible explanation is the ligation of a hydroxide (OH^-) ligand originating from a nearby water or due to the three-electron reduction of O_2. The experimental precedent for this model is the accumulation of the OH^--bound oxidized Ni-B state of the Ni-Fe active site in O_2-tolerant [NiFe] hydrogenases.[1,33–35] While this hypothesis does not directly involve the sidechain of Cys367, we believe its proximity to the open coordination site may be required for the efficacy of the transition to the H_{inact} state.

In a more recent study, Winkler et al. confirmed that the Cys367 could be structurally aberrant in *Cb*A5H.[36] The authors modeled X-ray diffraction data (PDB: 6TTL) of the aerobically crystallized *Cb*A5H with the Cys367 coordinating the H-cluster. Unfortunately, due to the poor resolution of the electron density, it is not possible to conclude with certainty whether the presented model is indeed the only possible fit, especially considering an unlikely long Fe_d-S(Cys367) distance of about 3.1 Å. For instance, the H_{inact}-SH state in *Dd*HydAB[14] has an Fe_d-SH distance of 2.4 Å. Our DFT calculations on the Cys-coordinated model of H_{inact} showed a very similar Fe-S(Cys) distance of 2.36 Å.[32] Unfortunately, the authors did not present a fit of the Fe_d-OH^- model to refute our second structural model of the H_{inact} state. Therefore, while the Cys-ligation to Fe_d would elegantly explain the process of inactivation, we believe further experimental validation is needed before drawing final conclusions about the structure of the H_{inact} state. Regardless of the exact inactivation mechanism, the structural peculiarity of Cys367 and the respective SCCP loop (see figure 1) seems unique to *Cb*HydA1 and *Cb*A5H. Therefore, it is tempting to suggest that this alternative configuration plays a role in the ability of *Cb*HydA1 (and *Cb*A5H) to access H_{inact}. Notably, Winkler et al. illustrated that a C367D amino acid substitution renders the respective variant of *Cb*A5H O_2-sensitive.[36]

Another surprising observation is the direct transition between the H_{ox} and the H_{inact} states without any observable intermediates in our spectroelectrochemical experiments.[32] In constrast, studies with *Dd*HydAB report the appearance of the intermediate (H_{trans}) state in the reductive activation of H_{inact}-SH to the H_{ox} state, suggesting two separate steps of inactivation (and reactivation): the electron transfer and the ligand dissociation (sulfide, in this case).[37] As a matter of fact, the transition from the H_{trans} state to the H_{ox} state in *Dd*HydAB requires a second $1e^-$ reduction. However, the electron acceptor for the second step is likely not the H-cluster as both the H_{trans} and the H_{ox} states of the H-cluster have the same S=1/2 spin state and thus are likely isoelectronic. The absence of the observable H_{trans} state in the case of *Cb*HydA1 suggests coupling of ligand binding and an electron transfer. As ligand binding is inherently slower than electron transfer, the H_{ox}-H_{inact} transition should be independent of the oxidizing potential. A recent study of inactivation kinetics in protein film voltammetry experiments supports this expectation.[36]

Because *Cb*HydA1 has bidirectional activity matching other [FeFe] hydrogenases,[31,32,36] it is unlikely the Cys367 retains the "off-H^+-pathway" configuration at all times. The Cys367-harboring flexible SCCP loop is more likely to be mobile and allow dynamic reorganization of the Cys367 sidechain. In line with this notion, Winkler et al. proposed a kinetic equilibrium between two (active) states in the electrochemical inactivation process in *Cb*A5H.[36] Intriguingly, Rutz et al.[38] have demonstrated enhanced electrochemical inactivation by making a near-surface M382E substitution in *Cb*HydA1. The authors proposed that such a modification increases protein mobility. If dynamic rearrangement of the protein environment around the H-cluster occurs, we must see evidence of that in the spectroscopic signatures of the active *Cb*HydA1. Therefore, we hypothesize that the oxidized, catalytically active (H_{ox}) state directly preceding the formation of the H_{inact} state must show some signs of such structural perturbation. To address this hypothesis, we performed a series of Electron Paramagnetic Resonance (EPR) and Fourier-transform Infrared (FTIR) spectroscopic experiments to uncover possible perturbations to the electronic structure of the H-cluster in the H_{ox} state. We also test a CO-inhibited variant of the H_{ox} state (H_{ox}-CO), which has the open coordination site of Fe_d occupied by carbon monoxide, excluding the possibility of binding an exogenous ligand, e.g., Cys367. Through the spectroscopic analysis, we show persuasive evidence that a structural heterogeneity indeed exists in the vicinity of the H-cluster.

RESULTS.

CW EPR experiments show spectral heterogeneity. In our EPR experiments on *Cb*HydA1 prepared at pH 7.5 in HEPES buffer, samples with the H_{ox} and the H_{ox}-CO states show two distinct spectral components each. In the case of the H_{ox} state, the two EPR signals have very similar principal g-values (see **figure 2**). In the case of the H_{ox}-CO state, the difference is much more dramatic. One of the EPR spectra (H_{ox}-CO(1)) resembles a signal of a $[3Fe4S]^{1+}$ cluster or a radical. Nonetheless, based on the pulse EPR measurements presented below, we are confident that the observed EPR signal originates from the CO-inhibited oxidized state of the H-cluster. The H_{ox}(2) and H_{ox}-CO(2) species are the two spectral forms most similar to the typical EPR spectra of H_{ox}, and H_{ox}-CO states observed in O_2-sensitive [FeFe] hydrogenases (see **table S1**). Note that the EPR spectra of the H_{ox} state also contain minor contributions from the H_{ox}-CO state with similar speciation to that of the pure H_{ox}-CO samples (see the simulation in **figure 2A**).

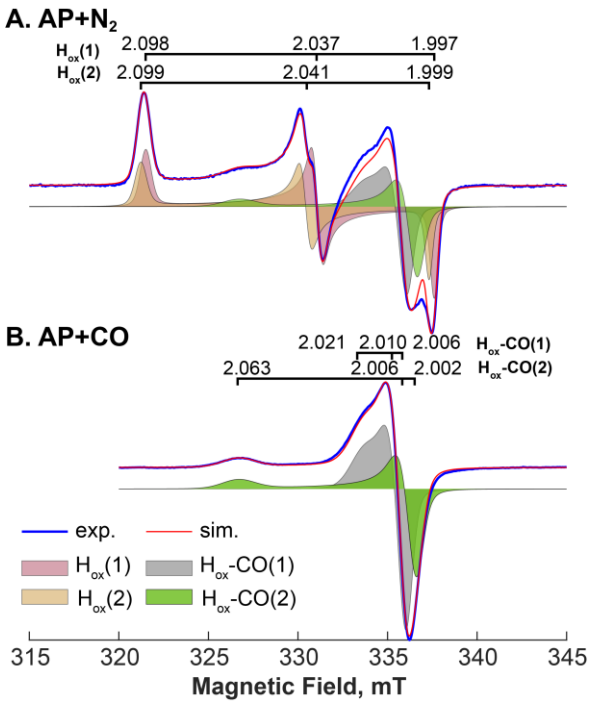

Figure 2. EPR spectra of the H_{ox} (A) and the H_{ox}-CO (B) states at pH 7.5 obtained by treating as-prepared (AP) sample of *Cb*HydA1 with N_2 and CO respectively. Blue traces are the experimental spectra measured at 40K. Red traces are the simulations using components depicted in shaded areas with the respective g-values presented above the spectra. Key experimental conditions: microwave frequency, 9.434 GHz; microwave power, 0.1 mW; modulation amplitude, 0.1 mT.

The two forms of either H_{ox} or H_{ox}-CO states have different power saturation behavior. The temperature-dependent power saturation measurements (see **figure S1**) model well with a combination of Orbach and Raman spin-lattice relaxation processes. The former dominates at lower temperatures and the latter at higher temperatures. The Δ parameter of the Orbach relaxation appears to be very similar between the two forms of the same state, suggesting that the alteration of relaxation behavior is not associated with a modification of spin-spin interactions within the H-cluster. Surprisingly, the values of Δ extracted are at least three-fold lower than expected based on commonly used exchange coupling constants for the H-cluster (see discussion in the supporting information). Given the absence of similar data on the O_2-sensitive enzymes, we can only speculate on the source of this discrepancy. A systematic investigation of the relaxation properties of the

H-cluster in various [FeFe] hydrogenases is necessary to understand this phenomenon fully. We plan to do such a study in the future.

Another crucial observation is that the speciation is pH-dependent. At neutral-to-low pH, EPR spectra are dominated by one form of the H_{ox} (i.e., $H_{ox}(1)$) and one form of the H_{ox}-CO (i.e., H_{ox}-CO(1)) states, while at high pH the two species of either of the states exist in roughly equal proportions (see **figure S2** and **table S2** in the supporting information). It is also important to note that the pH dependence is not entirely consistent and appears to change depending on the choice of the buffer (see **figure S3**). Noteworthy, the EPR spectral composition did not follow a monotonic trend when we varied buffers throughout the pH titration. However, the speciation persists regardless of the buffer, albeit in different proportions (see **table S2**). And so, these observations indicate that while pH plays a role, the origin of the speciation is not associated with an isolated protonation event of the H-cluster or a neighboring amino acid.

FTIR experiments exclude protonation of the H-cluster. To clarify the origin of the speciation of H_{ox} and H_{ox}-CO states, we performed a pH-dependence study by FTIR spectroscopy (see **figure 3**). Spectra shown in **figure 3** have been obtained from the same set of samples we used for EPR measurements shown in **figure S2**, i.e., using phosphate buffer. Remarkably, the positions of bands in the H_{ox} and the H_{ox}-CO states showed no detectable pH dependence. This result is highly intriguing, considering the dramatic change observed in the EPR spectra of the two H_{ox}-CO states.

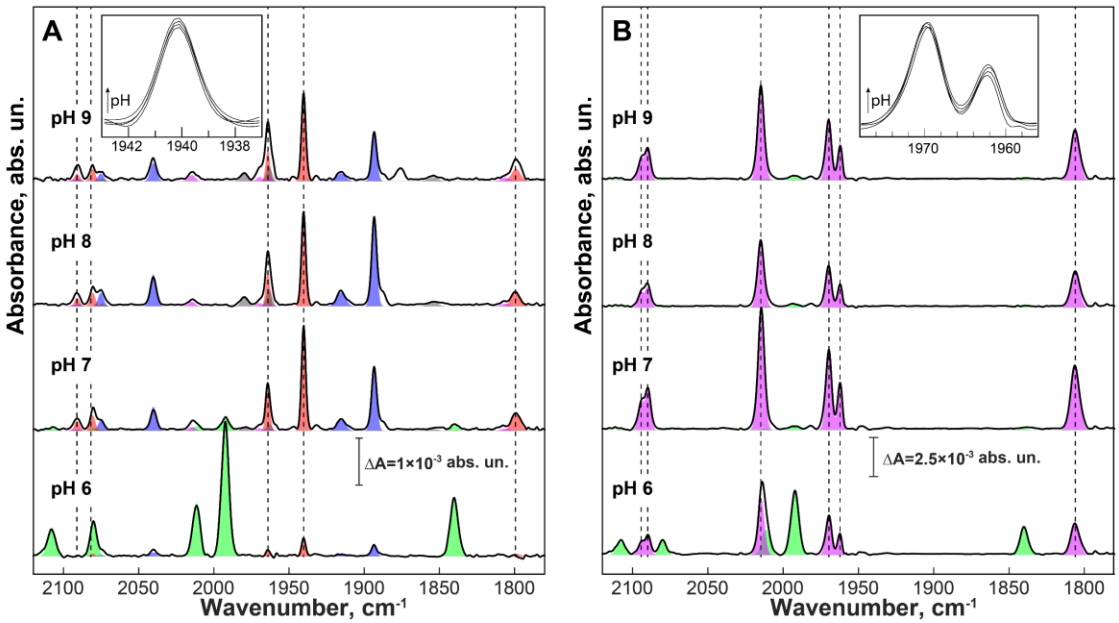

Figure 3. pH dependence of room-temperature FTIR spectra of *Cb*HydA1 prepared under 1 atm N_2 (A) or 1 atm CO (B) in phosphate buffer. Shaded areas are fits of bands assigned to various states of the H-cluster: green – H_{inact}, orange – H_{ox}, purple – H_{ox}-CO, blue – $H_{red}H^+$, grey – H_{hyd}. Dashed vertical lines indicate position of the CO and CN^- bands for the H_{ox} (A) and the H_{ox}-CO (B) states. Insets show a scaled overlay of selected bands.

Past studies have shown high sensitivity of the IR spectra to minute changes to the environment of the H-cluster.[39] Therefore, the absence of any pH-dependence in our IR experiments provides the first evidence *against* significant perturbation to the binuclear $[2Fe]_H$ subcluster due to protonation or pH-dependent binding of an additional ligand. Also, this result rules out protonation of the $[4Fe4S]_H$ cluster proposed for other [FeFe] hydrogenases as such an event should have a noticeable (4-7 cm^{-1}) shift in the IR spectra, well beyond the spectral resolution of the FTIR spectroscopy used.[40–42] Therefore, we can rule out any change

in the protonation state of the H_{ox} and the H_{ox}-CO states and the coordinating amino acids within the pH range used. By this exclusion, the pH and buffer dependence of the speciation in EPR observed must originate either from a secondary sphere or a more global structural modulation of the protein fold. Because buffer molecules may have a complex effect on the protein structure at different pH[43–46], we cannot provide any further details about this phenomenon. Future work employing molecular dynamic simulations and high-resolution structural methods may provide further insight.

It is also important to note that we could not test pH values lower than pH 7 in our EPR experiments as the samples automatically transitioned to the EPR-silent H_{inact} state without exogenous oxidants. According to the FTIR data, for the fully active *Cb*HydA1, changing from neutral to acidic pH resulted in a near complete inactivation of the enzyme, while in the case of the CO-inhibited sample, the conversion is roughly 60-70% (see **figure 3**). Notably, the resulting IR spectra of the H_{inact} state are identical between the two sets of experiments. This ability to transition to the H_{inact} state at low pH indicates the low redox potential for the H_{ox}-H_{inact} transition, which is in line with our previous observations of activation-inactivation hysteresis in protein film cyclic voltammetry measurements at low pH.[32]

Pulse EPR experiments on the H_{ox} states. To further understand the spectroscopic speciations and to provide a detailed description of the electronic structure of the $[2Fe]_H$ subcluster in *Cb*HydA1, we performed pulse EPR experiments in combination with site-specific isotope labeling of the H-cluster.

In the past, ^{13}C (CN^-) and ^{57}Fe hyperfine coupling constants have proven very sensitive to the spin distribution around the di-iron subcluster.[47–50] Following these past reports, we prepared samples that included either ^{13}CN or $[2^{57}Fe]_H$ isotope-labeled counterparts (see supporting information) and performed Hyperfine Sublevel Correlation spectroscopy (HYSCORE) experiments to extract respective hyperfine (HF) coupling constants.

Table 1. HF coupling constants of ^{13}C and ^{57}Fe nuclei. Numbers in parentheses are uncertainties in the least significant digit.

Site	HF coupling constants (MHz) (A_{xx}, A_{yy}, A_{zz})			Euler angles (deg)		
	H_{ox}					
$^{57}Fe_p$ [a,b]	-1.7(3)	11.8(3)	7.0(3)	42(5)	63(5)	-60(5)
$^{57}Fe_d$ [a,b]	16.0(5)	12.1(5)	16.8(5)	0(10)	0(10)	0(10)
$^{13}C_p$ [a,b]	4.1(2)	5.6(2)	5.5(2)	0(10)	0(10)	0(40)
$^{13}C_d$ [a,b]	30.5(5)	25.5(5)	27.0(5)	10(10)	20(10)	0(40)
	H_{ox}-CO					
$^{57}Fe_p$ [c]	6.0(5)	3.5(2)	0.0(5)	0(10)	20(5)	45(5)
$^{57}Fe_p$ [d]	6.5(5)	3.5(2)	0.0(5)	0(10)	5(5)	45(5)
$^{57}Fe_d$ [c]	3.4(2)	3.4(2)	-2.3(2)	n.d.	10(5)	0(10)
$^{57}Fe_d$ [d]	3.1(2)	2.4(5)	-2.4(2)	0(10)	26(5)	0(10)
$^{13}C_p$ [c,d]	8.5(2)	6.5(2)	7.5(2)	0(10)	0(10)	0(10)
$^{13}C_d$ [c,d]	3.5(2)	5.5(2)	5.5(2)	0(10)	0(10)	0(10)

[a]-form H_{ox}(1), [b]- H_{ox}(2), [c]- form H_{ox}-CO(1), [d]- form H_{ox}-CO(2).

In the case of the H_{ox} state, two ^{57}Fe HF interactions have been identified. The weaker coupling constant was determined in Q-band HYSCORE experiments (see **figure 4**), whereas the larger coupling is obtained from the line broadening of the CW EPR spectra. We could not differentiate the two different forms of the H_{ox} state in these experiments. A satisfactory fit to the CW EPR and ^{57}Fe HYSCORE data was obtained using an identical set of hyperfine coupling constants for the two H_{ox} species. However, the broad nature

of ^{57}Fe HYSCORE signals may obscure the speciation. Also, we found the ^{57}Fe HF coupling constants to be similar to those obtained for [FeFe] hydrogenase I from *Chlamydomonas reinhardtii* (*Cr*HydA1) by Rao and Britt.[50] The complete set of HF coupling constants extracted is presented in **table 1**.

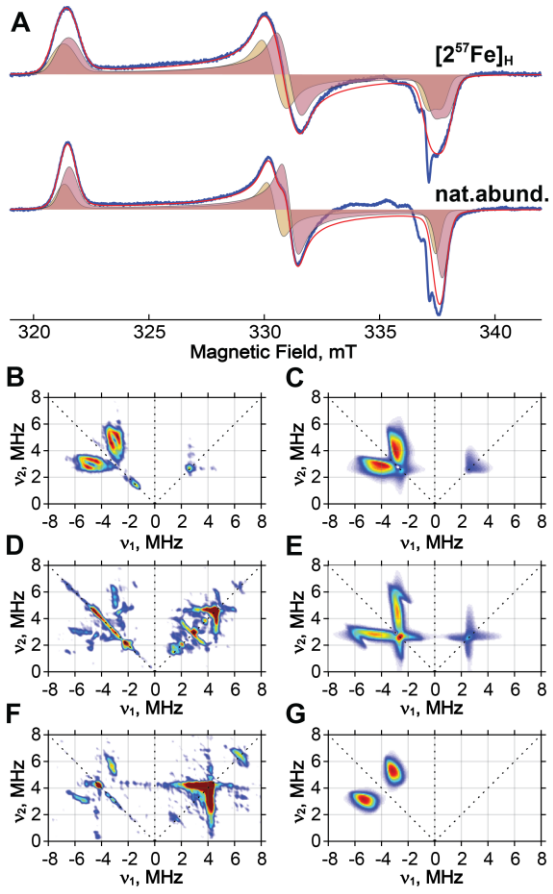

Figure 4. Study of ^{57}Fe HF interaction in the H_{ox} state of *Cb*HydA1. **A.** Effect of ^{57}Fe-isotope labeling on the line broadening of the CW X-band EPR spectra. Blue traces are experimental spectra of unlabeled and ^{57}Fe labeled samples of *Cb*HydA1, red traces are simulations using H_{ox} parameters $^{57}Fe_p$ and $^{57}Fe_d$ from **table 1**. **B,D** and **F** are Q-band HYSCORE spectra measured at g=2.10, 2.04 and 2.00 respectively. **C, E** and **G** are respective simulations accounting for $^{57}Fe_p$ from **table 1**. Key experimental conditions for A: temperature, 40 K; MW power, 0.1 μW; modulation amplitude, 0.3 mT; MW Frequency, 9.4354 GHz. Key experimental conditions for B-F: temperature, 20K; Magnetic field, 1158.0 mT(B), 1191.4 mT (D), 1217.2 mT(F); MW Frequency, 33.980 GHz (B,F), 34.045 GHz (D); t[π/2]=12 ns; τ=148 ns (B), 128 ns (D), 248 ns (F).

Next, we performed similar experiments on the ^{13}C-labeled samples. As expected, we identified two substantially different ^{13}C HF couplings in HYSCORE measurement of the ^{13}CN labeled *Cb*HydA1. Due to the exact cancelation effect, the X-band HYSCORE experiments are dominated by the smaller ^{13}C HF coupling, whereas the larger ^{13}C HF coupling dominates the Q-band HYSCORE experiments (see **figure 5** and **figures S4, S5** in the supporting information). Importantly, despite the narrow nature of the ^{13}C cross-

correlation ridges, we were not able to differentiate the two forms of H_{ox}. Therefore, even if there is a difference in the ^{13}C HF coupling constants between $H_{ox}(1)$ and $H_{ox}(2)$ species, it is within the error margins of determining the peak positions of the ^{13}C HF interactions (±0.2 MHz).

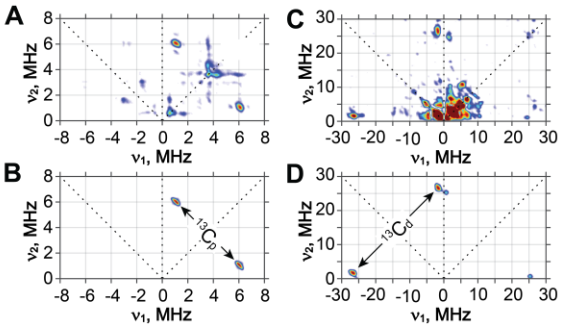

Figure 5. HYSCORE spectra of the H_{ox} state of ^{13}C-labeled *Cb*HydA1 measured at maximum absorption. **A.** X-band HYSCORE measurements at g=2.039. **C.** Q-band HYSCORE measurements at g=2.037. **B** and **D** are simulations of A and C respectively (see table 1). Experimental conditions can be found in the supporting information (figure **S5).**

Speciation aside, we also can conclude that the spin distribution in the $[2Fe]_H$ subcluster is strongly biased towards one of the iron sites, which is in line with most studies of O_2-sensitive [FeFe] hydrogenases. The close resemblance of the IR, EPR, and HYSCORE data to past studies on other systems allows us to assign the formal 1+ oxidation state to the distal iron. Consequently, we can conclude that in *Cb*HydA1, the H_{ox} state (regardless of the speciation) is characterized by a valence-localized $Fe(II)_p$-$Fe(I)_d$ core of the $[2Fe]_H$ subcluster similar to other [FeFe] hydrogenases.

Pulse EPR experiments on the H_{ox}-CO states. Unlike the case of the H_{ox} state, the two species of the H_{ox}-CO states observed can be separated based on the temperature dependence of the spin relaxation. The fast-relaxing H_{ox}-CO(2) species can only be observed in pulse EPR experiments at temperatures below 40K, optimally at 10-20K. At temperatures above 50-60K, pulse EPR spectra only show the H_{ox}-CO(1) species (see **figure S6**). It is important to note that, contrary to pulse EPR, the two forms can be detected in CW EPR spectra up to 140 K (see **figure S7**). Since traverse spin relaxation (T_2) governs the decay of signal in primary spin echo and free induction decay pulse sequences, we suggest that the temperature dependence of T_2 may play a role in the depletion of the H_{ox}-CO(2) signal in pulse experiments at high temperatures. Future investigation of the spin-relaxation of the H-cluster may provide a detailed explanation of this phenomenon. Nonetheless, taking advantage of this temperature behavior, we performed a series of HYSCORE measurements at low and high-temperature regimes to resolve ^{57}Fe and ^{13}C(CN) HF coupling constants separately for the two H_{ox}-CO forms. For a direct comparison, we chose the field positions of the HYSCORE measurements to match the orientation selectivity patterns for the H_{ox}-CO(1) and the H_{ox}-CO(2) EPR spectra.

Figure 6 shows ^{57}Fe HYSCORE spectra acquired near the $g_\perp$ and $g_\parallel$ values of the EPR spectra, along with the respective simulations. Both low- and high-temperature ^{57}Fe HYSCORE spectra show two distinct signals, one in the (++) quadrant and one in the (+-) quadrant, that correspond to a weaker and a stronger ^{57}Fe HF coupling, respectively. The observation of the ^{57}Fe signals from the $[2Fe]_H$ subcluster in the high-temperature measurements unequivocally confirms our assignment of the more-isotropic, slow-relaxing

EPR signal in the CO-treated *Cb*HydA1 to the H_{ox}-CO state, hence the name - H_{ox}-CO(1). The complete set of HYSCORE spectra is shown in the supporting material (see **figures S8** and **S9**). Comparing high- and low-temperature HYSCORE measurements, the position of the ^{57}Fe cross-correlation ridges appears to be very similar for the H_{ox}-CO(1) and H_{ox}-CO(2) forms.

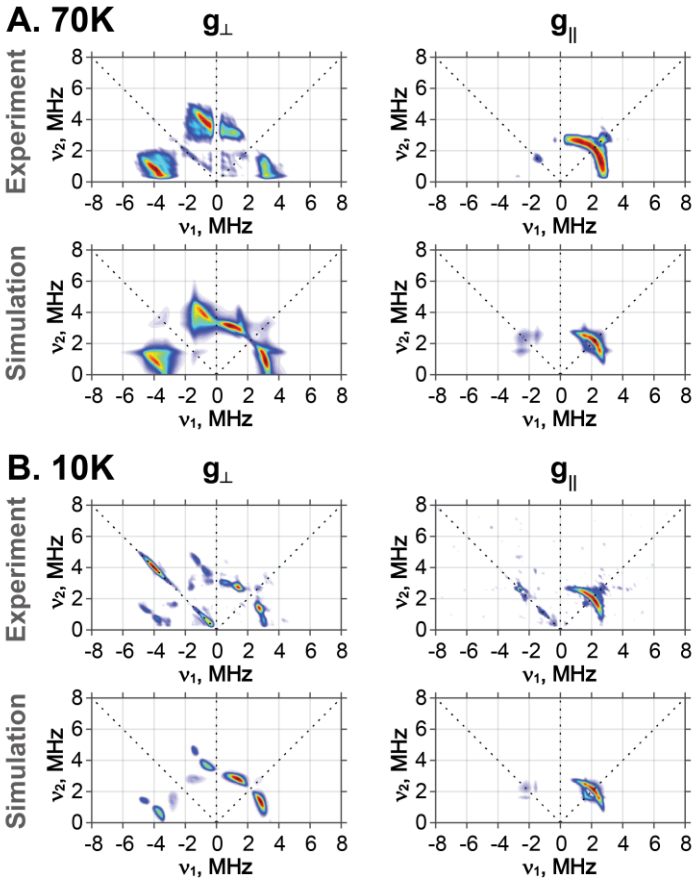

Figure 6. Field dependence of the ^{57}Fe HYSCORE spectra of high- and low-temperature species (A and B, respectively) together with the respective simulations using HF coupling constants from table 1 using H_{ox}-CO(1) parameters for A and H_{ox}-CO(2) parameters for B. Detailed experimental conditions are shown in **figure S8** of the supporting information.

Therefore, like the case of the H_{ox} state, simulations of both low- and high-temperature sets of HYSCORE spectra reveal similar ^{57}Fe HF coupling constants between the two forms of the H_{ox}-CO state. The differences in the extracted HF coupling constants are within the error margins of determination between H_{ox}-CO(1) and H_{ox}-CO(2) (see **table 1**)

To further understand the electronic structure of the $[2Fe]_H$ subcluster, we performed a HYSCORE study of the ^{13}C(CN) labeled *Cb*HydA1. Using X-band HYSCORE spectroscopy, we identified two ^{13}C HF coupling constants in low- and high-temperature measurements, once again confirming our assignment of H_{ox}-CO(1) to the CO-inhibited oxidized state of the H-cluster. Due to the position of the signals in HYSCORE spectra, two different blind-spot-defining τ-values were required to observe either the weaker or the stronger ^{13}C HF interaction. The complete set of orientation-selective HYSCORE spectra can be found in the supporting information (see **figures S10** and **S11**). **Figure 7** shows the representative ^{13}C HYSCORE spectra measured near the $g_\perp$ position of the respective CW EPR spectra. As can be seen in

Figure 7, the two species show near-identical positions of the ^{13}C signals. The simulations presented in **figures S10** and **S11** for H_{ox}-CO(2) and H_{ox}-CO(1) were performed using an identical set of ^{13}C HF coupling constants.

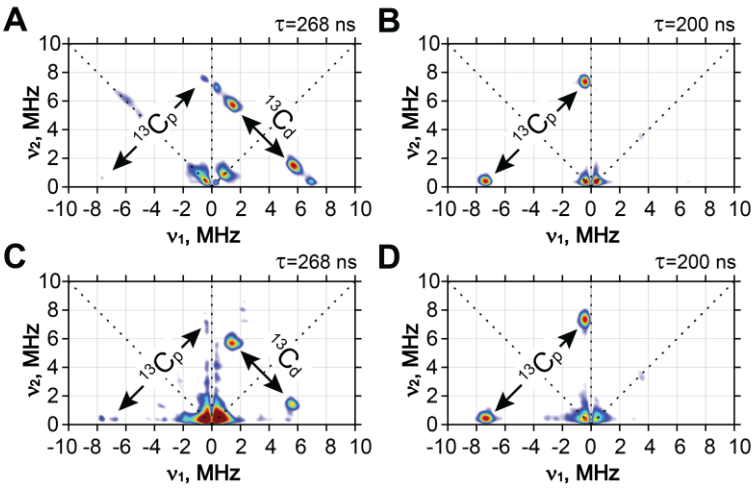

Figure 7. ^{13}C HYSCORE spectra of ^{13}C(CN)-labeled *Cb*HydA1, measured at 15 K (A, B) and 70 K (C,D). Simualtions and experimental conditions can be found in the supporting information (**figure S10** and **S11)**

Given the drastic difference in the CW EPR spectra of the two forms, the similarity of ^{57}Fe and ^{13}C HYSCORE signals for H_{ox}-CO(1) and H_{ox}-CO(2) is staggering. Together with similar observations for the two forms of the H_{ox} state, these results unequivocally show that the spectral speciation is not associated with a modulation of the electronic structure of the $[2Fe]_H$ subcluster whatsoever.

DISCUSSION

On the identity of the EPR-active species. The combination of FTIR, EPR, and HYSCORE studies presented above conclusively show that the two rhombic EPR signals of the N_2-treated sample are of the "H_{ox}" nature, and the two near-axial EPR signals of the CO-treated *Cb*HydA1 are of the "H_{ox}-CO" nature. The two EPR forms of the H_{ox} state exhibit similar g-anisotropies but differ in their temperature dependence of the spin relaxation behaviours. The two EPR forms of the H_{ox}-CO state have very different g-anisotropies and substantially different relaxation behavior. The fast-relaxing EPR signal H_{ox}-CO(2)) resembles the typical H_{ox}-CO state observed in many O_2-sensitive [FeFe] hydrogenases (see **table S1**). The slow-relaxing H_{ox}-CO form (H_{ox}-CO(1)) has a substantially narrower spectrum, with the high-temperature relaxation behavior more reminiscent of an organic radical than that of a metallocofactor. We investigated the two H_{ox}-CO forms separately by taking advantage of the differences in the relaxation behavior. The surprising similarity of the ^{57}Fe and ^{13}C HF coupling constants in the high- and low-temperature measurements unequivocally confirms that the two EPR forms originate from similar CO-inhibited states. This result simultaneously demonstrates that the speciation is not associated with any noticeable perturbations to the structure of the $[2Fe]_H$ subcluster either by varying ligand binding, varying interaction with a small molecule, e.g., proposed interaction with chloride[51], protonation of the *adt* bridge[40] or rearrangement of the CO and CN^- ligands proposed earlier[52,53].

While we are confident in our assignment, it is intriguing to find that the H_{ox}-CO(1) EPR spectrum is very similar to that of the radical-like signal ($R^{\bullet ox}$) proposed recently by Heghmanns et al. for *Cb*A5H.[54] The

authors observed $R^{\bullet ox}$ in EPR after exposing *Cb*A5H to O_2 while detecting predominantly the H_{inact} state by FTIR. The authors also reported strong ^{57}Fe HF interactions in the $[4^{57}Fe4S]_H$ subcluster and suggested the proximity of the postulated $R^{\bullet ox}$ radical to the H-cluster. The extracted ^{57}Fe coupling constants resembled that of the H_{ox}-CO state observed earlier for *Dd*HydAB and *Cr*HydA1.[47,50] We attempted to repeat similar experiments with *Cb*HydA1. However, just as we reported earlier,[32] *Cb*HydA1 exposed to air exhibited only a comparatively minor EPR signal typical for a $[3Fe4S]^{1+}$ cluster similar to that observed in apo-*Cb*HydA1 lacking the $[2Fe]_H$ subcluster (see **figure S12**). Therefore, we can only speculate on the nature of $R^{ox\bullet}$, and whether it is a result of a specific sample preparation procedure used by Heghmanns et al.[54] It cannot be excluded that the lack of $R^{ox\bullet}$ in the H_{inact} state in our experiments is due to differences in the strains of *Clostridium beijerinkii* used. However, as the amino acid sequences for *Cb*HydA1 and *Cb*A5H only differ by a couple of residues (see **figure S13**), we consider this scenario unlikely. Another possibility is the incomplete O_2-dependent inactivation of *Cb*A5H, resulting in a residual H_{ox}-CO(1) signal. The low spin concentrations of <0.1 spins/mol quoted by the authors for $R^{ox\bullet}$ are in line with such a scenario. If that is the case, it may suggest that either H_{ox}-CO(1) is more resilient to (over)oxidation to H_{inact} than H_{ox}-CO(2) or that H_{ox}-CO(2) may be more prone to oxidative damage upon reacting with O_2 since both *Cb*A5H and *Cb*HydA1 show lower activity after reactivation.[32,54] We putatively assign the $R^{ox\bullet}$ species to H_{ox}-CO(1), but further experiments are needed to fully understand the relationship between $R^{ox\bullet}$ and H_{ox}-CO(1).

Furthermore, the ^{13}C and ^{57}Fe HF coupling constants observed in the H_{ox} and H_{ox}-CO states here are very similar to those observed in the *Clostridium pasteurianum* hydrogenase I (*Cp*HydA1 or *Cp*I) and *Cr*HydA1, indicating that the electronic structure of the $[2Fe]_H$ subcluster in *Cb*HydA1 is very similar to that of O_2-sensitive [FeFe] hydrogenases. Therefore, it is unlikely that peculiarities of the electronic structure of the $[2Fe]_H$ subcluster in *Cb*HydA1 play roles in the ability of the enzyme to access the H_{inact} state.

Speciation is not associated with a modification to the charge distribution, or the spin-spin interactions of the H-cluster. The temperature-dependent power saturation study provides another important piece of information. The Orbach relaxation parameter Δ is the energy gap between the ground and the first excited spin state of the H-cluster. As discussed in the supporting information, the Δ parameter depends on the spin-spin interactions within the five-spin system of the H-cluster. The fact that a very similar Δ parameter characterizes the two EPR forms of H_{ox} and, separately, the two EPR forms of H_{ox}-CO is an indication of little-to-no variation in the spin-spin interactions within the H-cluster for either of the states. This rules out a possibility of a major reorganization of the spin-spin interactions between the components of the six-iron cofactor. The absence of any substantial alterations to the ^{13}C and ^{57}Fe HF coupling constants among two forms of the same state also supports this conclusion. Logically, this leaves us with the only possible conclusion: the speciation observed in EPR spectra is due to the local perturbations to the Fe sites in the $[4Fe4S]_H$ subcluster *without* a significant effect on the overall spin-state of the H-cluster.

We now discuss how these local perturbations are manifest in *Cb*HydA1. Due to a complete invariance of the FTIR spectral components to changes in pH, we argue against any change in the protonation state of coordinating amino acids. Senger et al. proposed a protonation of one of the cysteines of the $[4Fe4S]_H$ subcluster at acidic pH in O_2-sensitive [FeFe] hydrogenases by the blue shift of CN^- and CO bands in ATR-FTIR spectra of the H_{ox} state.[40,41] While there is a debate about the interpretation of experimental data,[42] DFT calculations by Senger et al.[40] consistently predict a well-resolved shift of more than 4 cm^{-1} for CN^- and CO stretching bands upon protonation of Cys ligands of the $[4Fe4S]_H$ subcluster. The absence of any noticeable pH-dependent shifts in our IR experiments, thus, attests strongly against such a possibility.

We also argue against any significant ligand or charge distribution modification of the H-cluster. Rodríguez Maciá et al. illustrated a dependence of the IR band positions on the redox state of nearby accessory FeS

clusters, highlighting an exceptional sensitivity of IR spectra of the H-cluster to changes in its environment.[39] Therefore, we argue against any significant ligand or charge distribution modification of the H-cluster as a cause of the speciation observed in EPR. Consequently, we conclude that the chemical composition of the H-cluster is the same for the $H_{ox}(1,2)$ forms and the H_{ox}-CO(1,2) forms.

As we also argue against any significant modification to the spin state of the H-cluster (see above), the only remaining plausible explanation of the speciation is a *geometric* perturbation to the Cys-ligands of the H-cluster.

Electronic structure of the H-cluster. To provide further insight, we must evaluate whether a change in the local symmetry of the Fe ions in the $[4Fe4S]_H$ cubane can explain the observed differences in the g-values of EPR spectra of two forms of the same state. An accurate prediction of g-values in multi-spin metallocofactors by quantum chemical calculations is prohibitively challenging. However, for this work, it is sufficient to consider the relationship between observed and intrinsic g-values resulting from the spin-spin exchange coupling network (see commentary to Figure S1 in the supporting information for a detailed overview).

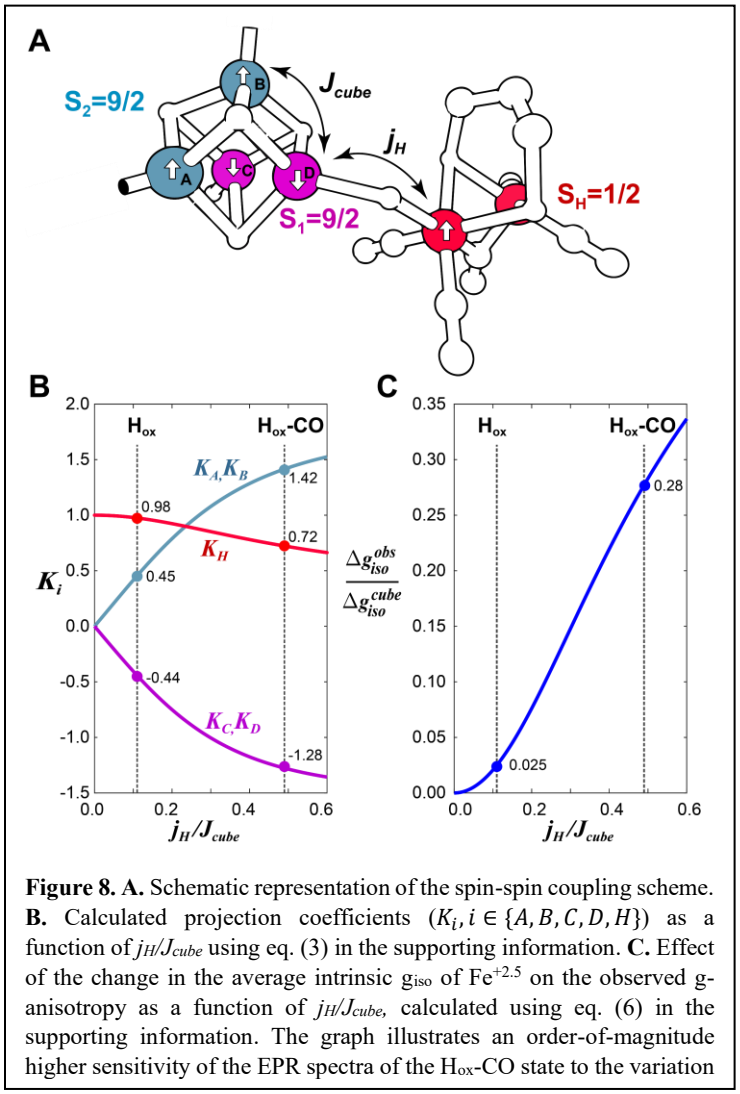

Figure 8. A. Schematic representation of the spin-spin coupling scheme. **B.** Calculated projection coefficients ($K_i, i \in \{A, B, C, D, H\}$) as a function of j_H/J_{cube} using eq. (3) in the supporting information. **C.** Effect of the change in the average intrinsic g_{iso} of $Fe^{+2.5}$ on the observed g-anisotropy as a function of j_H/J_{cube}, calculated using eq. (6) in the supporting information. The graph illustrates an order-of-magnitude higher sensitivity of the EPR spectra of the H_{ox}-CO state to the variation

In a nutshell, the $[4Fe4S]_H^{2+}$ subcluster is best described as a system of two valence-delocalized Fe^{+2}-Fe^{+3} pairs (commonly called a $Fe^{+2.5}$-$Fe^{+2.5}$ pair).[55,56] The ferromagnetic coupling within the pair leads to the ground state $S_{pair} = 9/2$. Strong antiferromagnetic coupling between spins of $Fe^{+2.5}$-$Fe^{+2.5}$ pairs leads to the singlet ($S_{cube,1} = 0$) ground state and $S_{cube,2} = 1$ first excited state of $[4Fe4S]_H^{2+}$. The average coupling constant is designated as J_{cube} (see **figure 8A**). The $[2Fe]_H$ subcluster is described as a mixed-valence pair of low-spin Fe ions (Fe^{+1}-Fe^{+2}) with a somewhat delocalized $S_H = 1/2$ unpaired spin.[48,50,57] The spin-spin exchange coupling (j_H) between Fe_D and the $S_H = 1/2$ mixes the ground singlet $|S_{cube} = 0\rangle$ state and the excited triplet $|S_{cube} = 1\rangle$ state of the $[4Fe4S]_H$ subcluster.[58,59] The resulting $S_g = 1/2$ ground state of the H-cluster is a mixture of $[2Fe]_H$-based and $[4Fe4S]_H$-based spin wavefunctions. $K_i = \langle s_{iz}\rangle/\langle S_z\rangle$ are spin projection coefficients that report on the mixing; $\langle s_{iz}\rangle$ are the expectation values for the individual spins ($i \in A, B, C, D, H$, see **figure 8**A,B). Consequently, ^{57}Fe Mössbauer and EPR measurements report non-zero effective spin population on the Fe sites of the formally diamagnetic $[4Fe4S]_H$ subcluster.[47,57,60] The larger the j_H/J_{cube} ratio, the stronger the effective HF coupling constants originating from the $[4Fe4S]_H$ subcluster, including that of the β-protons of Cys ligands.[57] Based on the known ^{57}Fe HF coupling constants in the $[4Fe4S]_H$ subcluster,[47,50,60,61] it is possible to estimate the j_H/J_{cube} ratio to be 0.11 and 0.49 for H_{ox} and H_{ox}-CO respectively (see **figure 8B**, see SI for more details). The apparent g-tensor of the H-cluster is a linear combination of the local (site) g-tensors ($\boldsymbol{g_i}$) of the individual spins scaled by the spin projection factors: $\boldsymbol{g^{obs}} = \sum_i K_i \boldsymbol{g_i}$. Figure 8B shows the relevant constants calculated using equations shown in the supporting information.

The exact anisotropy and orientation of the local g-tensors are unknown. Thus, a reliable analysis can only be performed on the isotropic component of the local and apparent g-tensors ($g_{iso} = (g_x + g_y + g_z)/3$). The relationship between the two can be approximated as $g_{iso}^{obs} = \left(2K_{A,B} + 2K_{C,D}\right)g_{iso}^{cube} + K_H g_{iso}^{H}$, assuming identical $g_{iso}^{cube} = g_{iso}(Fe^{+2.5})$ for all four Fe sites of the $[4Fe4S]_H$ subcluster (due to symmetry considerations, seesupporting information). In a strong double exchange limit, g_{iso}^{cube} is an average of intrinsic $g_{iso}(Fe^{+2})$ and $g_{iso}(Fe^{+3})$.[62–64] g_{iso}^{H} is the local g-value of the $S_H = 1/2$ $[2Fe]_H$ subcluster that is largely unknown. Since all our experimental data suggest no alterations to the electronic structure of the $[2Fe]_H$ subcluster, we can assume that g_{iso}^{H} values are effectively the same for the two spectral forms of the H_{ox} and the H_{ox}-CO states. Furthermore, we can consider the spin-projection factors (K_i) effectively invariant to speciation since the Δ factor of the Orbach relaxation and the ^{13}C, ^{57}Fe HF coupling constants are very similar for the two forms of the same state. Using these assumptions, we can estimate the average deviation of the intrinsic g-values of Fe sites (Δg_{iso}^{cube}) in the $[4Fe4S]_H$ subcluster based on the variation in the g-values of the observed EPR forms (Δg_{iso}^{obs}). The ratio between the two as a function of the j_H/J_{cube} ratio is shown in **figure 8C**. The two H_{ox}-CO states differ in g_{iso} by $\Delta g_{iso}^{obs}(\mathrm{H_{ox}\text{-}CO}) = 0.012 \pm 0.002$ and so we estimate that the g_{iso}^{cube} value for the two EPR forms of H_{ox}-CO differ by $\Delta g_{iso}^{cube}(\mathrm{H_{ox}\text{-}CO}) = 0.043 \pm 0.006$. In the case of the H_{ox} state, $\Delta g_{iso}^{obs}(\mathrm{H_{ox}}) = 0.0023 \pm 0.001$ and thus $\Delta g_{iso}^{cube}(\mathrm{H_{ox}}) = 0.09 \pm 0.04$. Overall, considering the error margins in our estimations, the two EPR species of the H_{ox} and the H_{ox}-CO states are likely to have similar variations in the average intrinsic g_{iso}^{cube} by

$$\Delta g_{iso}^{cube} \cong 0.04 - 0.09.$$

Experimental estimates of $g_{iso}(Fe^{+2.5})$ in $[4Fe\text{-}4S]^{2+}$ clusters are not available due to the typically diamagnetic nature of the cofactors. Therefore, we consider precedents from mono-nuclear, non-heme Fe systems instead. A deviation of $g_{iso}(Fe^{+2.5})$ from the free electron $g_e = 2.0023$ due to spin-orbit coupling is expected to be in between that of ferric and ferrous ions, with the latter (typically) exhibiting a larger divergence.[62] To our knowledge, the largest reported variation in $g_{iso}(Fe^{+2})$ due to structural perturbation

is observed in the C42S and C9S variants of Fe^{2+} rubredoxin from *Clostridium pasteurianum* by Yoo et al.[65] Both of the studied variants showed two spectroscopic forms, A and B, with $g_{iso}(A) = 2.0267$ and $g_{iso}(B) = 2.1033$, i.e., $\Delta g_{iso}(Fe^{+2}) = 0.0766$. Unfortunately, the authors did not resolve exact nature of the structural perturbations causing such a difference in g-values. More direct structural insight can be gained from the study of flexible $[Fe(C_3S_5)_2]^{2-}$ complexes by Zadrozny et al.[66] A variation in the core $[Fe^{2+}S_4]$ ligand geometry for different salts significantly impacted the g-values of the Fe^{2+} ion. The authors observed that a twist of two $[C_3S_5]$ ligand planes by 10-15° off the orthogonal arrangement coincides with a substantial change in the character of the g-tensor with $\Delta g_{iso}(Fe^{2+}) \cong 0.03 - 0.07$. Since Δg_{iso} in these studies are on par with our estimations, this comparison validates our notion that a conformational variation in the local environment of the $[4Fe4S]_H$ cluster is sufficient to cause noticeable changes in the observed g-values.

To corroborate such a possibility, we performed ^{1}H Electron Nuclear Double Resonance (ENDOR) experiments on the H_{ox}-CO state. Strong inter-subcluster exchange (j_H) in this state results in the dominant contribution of $[4Fe4S]_H$-based spin wavefunctions to the spin ground state (see figure 8B). Consequently, signals from the β-protons on the Cys ligands of the $[4Fe4S]_H$ dominate the ^{1}H ENDOR spectra.[57] As ^{1}H HF coupling constants are highly sensitive to the relative orientation of Cys-S ligands [67–69], such spectra are good reporters of structural perturbations of the coordination environment of [4Fe4S] clusters. Indeed, a direct comparison of ^{1}H ENDOR spectra of H_{ox}-CO(1) and H_{ox}-CO(2) forms shows substantial differences (see **figure S14**), validating a structural reorganization of the S-Cys ligands to the $[4Fe4S]_H$ cluster from one EPR form to the other. Unfortunately, detailed analysis of such spectra has a large uncertainty due to the broad nature of underlying spectral components. Extracting structural metrics from the perturbations observed requires measurements on single-crystal protein samples.[69,70] Generation of such samples of *Cb*HydA1 has been, so far, largely unsuccessful. TRIPLE or liquid-state paramagnetic NMR may be promising alternative methodologies to explore in the future in conjunction with advanced quantum chemical computations.

Nature of structural heterogeneity in *Cb*HydA1. Information about the structural mobility of the protein environment of the H-cluster in [FeFe] hydrogenases is very limited. To our knowledge, the only applicable experimental precedent is the work of Artz et al. on the O_2-sensitive enzyme *Cp*HydA1 (historically known as *Cp*I).[15] Using high-resolution X-ray crystallography, the authors have illustrated conformational heterogeneity of two amino acids neighboring the H-cluster, Ser357, and Met353, and proposed a role for amino acid mobility on the catalytic bias of *Cp*HydA1.[15] Based on the structure (PDB: 6N59), Ser357 can directly interact with one of the $[4Fe4S]_H$-binding cysteines while Met353 is in proximity to the bridging CO ligand of the $[2Fe]_H$ subcluster. While we can rule out an identical effect to be at play in *Cb*HydA1 since Ala425 is in the Ser357-equivalent position, it is important to note that no structure-linked speciation of EPR spectra of the H_{ox} and H_{ox}-CO states have ever been reported for *Cp*HydA1. The authors justifiably proposed redox-dependent conformational changes rather than a dynamic rearrangement.

To formulate a hypothesis, we compared the environment of the $[4Fe4S]_H$ of the aforementioned structure of *Cp*HydA1 with that of air-exposed *Cb*A5H (PDB 6TTL).[36] Since the former represents a typical structure of the active enzyme and the latter represents the divergent structure associated with the H_{inact} state, this comparison approximates the possible structural mobility in *Cb*A5H and *Cb*HydA1. As seen in **figure 9**, the positioning of the loops and helices bearing three coordinating cysteines (Cys423, Cys571, and Cys567 for *Cb*HydA1) match very closely for the two structures. This suggests that these protein regions are not markedly mobile or even differ from system to system. On the other hand, the conserved $SC_{367}CP$ loop bearing the Cys367 and Cys368 is noticably different between the two structures, which suggests potential mobility as was, in fact, proposed by Winkler et al.[36] and, most recently, by Rutz et al.[38]

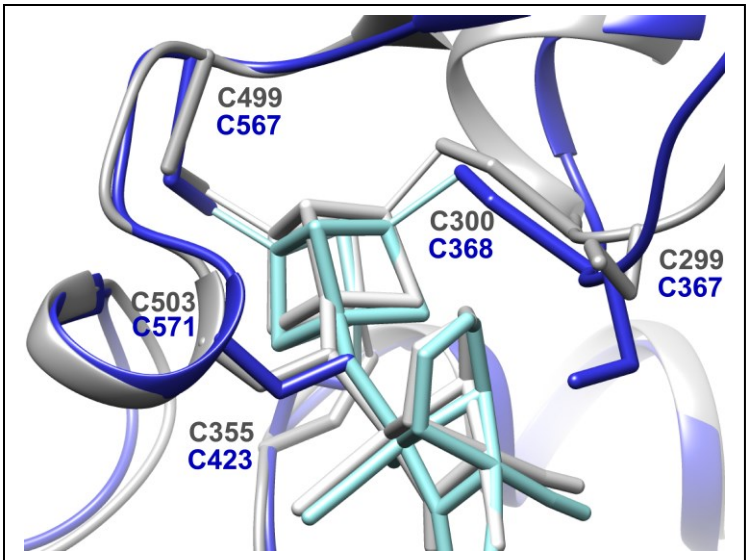

Figure 9. Comparison of the coordination environment of the [4Fe4S] cluster. Gray – structure of *Cp*HydA1 (PDB: 6N59), Blue and Cyan – structure of *Cb*A5H (PDB: 6TTL)

We could not find any other substantial divergence in the environment of the $[4Fe4S]_H$ subcluster. Therefore, the scenario in which the motion of the SCCP loop allows for a considerable alteration of the $[4Fe4S]_H$ ligand geometry appears to be the most reasonable explanation of the observed speciation, at least given the available structural data. Consequently, we propose that the exsistence of two spectral forms of the H_{ox} and the H_{ox}-CO states in EPR is the hallmark of the structural heterogeneity of the SCCP loop. It remains to be seen whether this phenomenon is associated with a rapid switch between at least two distinct conformations or a continuous mobility with two (or more) potential minima. Our EPR analysis is of frozen-solution samples, so we have no definitive way of discriminating the two possibilities.

Further crystallographic and spectroscopic experiments are needed to provide structural details of the observed phenomenon. Nonetheless, the work presented here provides the first experimental evidence for the existence of structural mobility of the H-cluster environment in *Cb*HydA1. Because the $H_{ox}(2)$ and the H_{ox}-CO(2) forms almost completely vanish at mildly acidic conditions that promote (auto)inactivation, it is tempting to suggest that adapting to an inactivation-favorable confirmation is required prior to the transition to H_{inact}. If true, then the two interchanged states preceding H_{inact} suggested by Winkler et al. would be the $H_{ox}(2)$ and the $H_{ox}(1)$ states (see scheme 1 below).

Scheme 1.

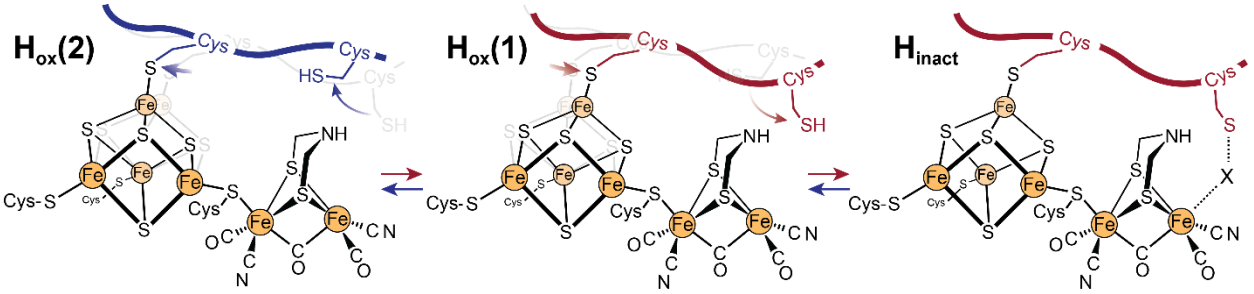

CONCLUSIONS

In this work, we applied EPR and FTIR spectroscopy to investigate the active oxidized state (H_{ox}) of *Cb*HydA1 and its CO-adduct (H_{ox}-CO). Using CW EPR measurements, we observed two forms of both states. HYSCORE and FTIR investigation of the electronic structure of the H-cluster reveal no alterations to the coordination environment of the $[2Fe]_H$ subcluster that would explain such spectral speciation. These results also exclude the possibility of an intermittent weak interaction between the distal Fe site and the S-Cys367 in the active H-cluster. Furthermore, we conclude that the electronic structure of $[2Fe]_H$ is highly similar between *Cb*HydA1 and previously studied O_2-sensitive [FeFe] hydrogenases. Based on the invariance of FTIR bands associated with the H_{ox} and the H_{ox}-CO states to pH, we exclude the protonation of the H-cluster either at the $[2Fe]_H$ or the $[4Fe4S]_H$ subcluster, at least in the pH-range studied. By exclusion, the extensive analysis presented here allows us to conclude that a structural modulation of the environment of the $[4Fe4S]_H$ subcluster is the cause of speciation. Therefore, we conclude that the observations of two (iso)forms of the oxidized states of the H-cluster in EPR report on the unusual mobility of the environment of the active center of *Cb*HydA1. To our knowledge, such a spectroscopic phenomenon is unprecedented in O_2-sensitive [FeFe] hydrogenases; and so we suggest that the structural heterogeneity uncovered here is linked to the ability of *Cb*HydA1 to transition to the O_2-protected state. Consequently, we propose a rapid switch between protein conformations in the vicinity of the H-cluster, one of which allows the bidirectional activity of the enzyme while the other promotes transition to the inactive state under oxidizing conditions.

SUPPORTING INFORMATION

Materials and methods; review of relevant spin-spin exchange formalisms; temperature dependence of CW EPR power saturation together with a commentary; supplementary EPR, HYSCORE and ENDOR figures and related tables; amino acid sequence alignment of *Cb*HydA1 and *Cb*A5H.

ACKNOWLEDGMENTS

We thank Dr. James Birrell (MPI-CEC, Germany) and Dr. Thomas Rauchfuss (University of Illinois, Urbana-Champaign, IL) for providing us with the ^{57}Fe-labeled synthon. This material is based upon work supported by the U.S. Department of Energy, Office of Science, Office of Basic Energy Sciences program under Award Number DE-SC0018087 and by the National Science Foundation under Award Number CHE-1943748.

REFERENCES

(1) Lubitz, W.; Ogata, H.; Rüdiger, O.; Reijerse, E. Hydrogenases. *Chem. Rev.* **2014**, *114* (8), 4081–4148. https://doi.org/10.1021/cr4005814.
(2) Wittkamp, F.; Senger, M.; Stripp, S. T.; Apfel, U.-P. [FeFe]-Hydrogenases: Recent Developments and Future Perspectives. *Chem. Commun.* **2018**, *54* (47), 5934–5942. https://doi.org/10.1039/C8CC01275J.
(3) Birrell, J. A.; Rodríguez-Maciá, P.; Reijerse, E. J.; Martini, M. A.; Lubitz, W. The Catalytic Cycle of [FeFe] Hydrogenase: A Tale of Two Sites. *Coord. Chem. Rev.* **2021**, *449* (214191), 1–23. https://doi.org/10.1016/j.ccr.2021.214191.
(4) Morra, S. Fantastic [FeFe]-Hydrogenases and Where to Find Them. *Front. Microbiol.* **2022**, *13* (853626), 1–8. https://doi.org/10.3389/fmicb.2022.853626.

(5) Hambourger, M.; Gervaldo, M.; Svedruzic, D.; King, P. W.; Gust, D.; Ghirardi, M.; Moore, A. L.; Moore, T. A. [FeFe]-Hydrogenase-Catalyzed H_2 Production in a Photoelectrochemical Biofuel Cell. *J. Am. Chem. Soc.* **2008**, *130* (6), 2015–2022. https://doi.org/10.1021/ja077691k.
(6) Melis, A.; Zhang, L.; Forestier, M.; Ghirardi, M. L.; Seibert, M. Sustained Photobiological Hydrogen Gas Production upon Reversible Inactivation of Oxygen Evolution in the Green Alga *Chlamydomonas reinhardtii*. *Plant Physiol.* **2000**, *122* (1), 127–136. https://doi.org/10.1104/pp.122.1.127.
(7) Avilan, L.; Roumezi, B.; Risoul, V.; Bernard, C. S.; Kpebe, A.; Belhadjhassine, M.; Rousset, M.; Brugna, M.; Latifi, A. Phototrophic Hydrogen Production from a Clostridial [FeFe] Hydrogenase Expressed in the Heterocysts of the Cyanobacterium Nostoc PCC 7120. *Appl. Microbiol. Biotechnol.* **2018**, *102* (13), 5775–5783. https://doi.org/10.1007/s00253-018-8989-2.
(8) Wegelius, A.; Khanna, N.; Esmieu, C.; Barone, G. D.; Pinto, F.; Tamagnini, P.; Berggren, G.; Lindblad, P. Generation of a Functional, Semisynthetic [FeFe]-Hydrogenase in a Photosynthetic Microorganism. *Energy Environ. Sci.* **2018**, *11* (11), 3163–3167. https://doi.org/10.1039/C8EE01975D.
(9) Magnuson, A.; Mamedov, F.; Messinger, J. Toward Sustainable H_2 Production: Linking Hydrogenase with Photosynthesis. *Joule* **2020**, *4* (6), 1157–1159. https://doi.org/10.1016/j.joule.2020.05.014.
(10) Calusinska, M.; Happe, T.; Joris, B.; Wilmotte, A. The Surprising Diversity of Clostridial Hydrogenases: A Comparative Genomic Perspective. *Microbiology* **2010**, *156* (6), 1575–1588. https://doi.org/10.1099/mic.0.032771-0.
(11) Søndergaard, D.; Pedersen, C. N. S.; Greening, C. HydDB: A Web Tool for Hydrogenase Classification and Analysis. *Sci. Rep.* **2016**, *6* (34212), 1–8. https://doi.org/10.1038/srep34212.
(12) Land, H.; Sekretareva, A.; Huang, P.; Redman, H. J.; Németh, B.; Polidori, N.; Mészáros, L. S.; Senger, M.; Stripp, S. T.; Berggren, G. Characterization of a Putative Sensory [FeFe]-Hydrogenase Provides New Insight into the Role of the Active Site Architecture. *Chem. Sci.* **2020**, *11* (47), 12789–12801. https://doi.org/10.1039/D0SC03319G.
(13) Furlan, C.; Chongdar, N.; Gupta, P.; Lubitz, W.; Ogata, H.; Blaza, J. N.; Birrell, J. A. Structural Insight on the Mechanism of an Electron-Bifurcating [FeFe] Hydrogenase. *eLife* **2022**, *11* (e79361), 1–20. https://doi.org/10.7554/eLife.79361.
(14) Rodríguez-Maciá, P.; Galle, L. M.; Bjornsson, R.; Lorent, C.; Zebger, I.; Yoda, Y.; Cramer, S. P.; DeBeer, S.; Span, I.; Birrell, J. A. Caught in the H_{inact} : Crystal Structure and Spectroscopy Reveal a Sulfur Bound to the Active Site of an O_2-stable State of [FeFe] Hydrogenase. *Angew. Chem. Int. Ed.* **2020**, *59* (38), 16786–16794. https://doi.org/10.1002/anie.202005208.
(15) Artz, J. H.; Zadvornyy, O. A.; Mulder, D. W.; Keable, S. M.; Cohen, A. E.; Ratzloff, M. W.; Williams, S. G.; Ginovska, B.; Kumar, N.; Song, J.; McPhillips, S. E.; Davidson, C. M.; Lyubimov, A. Y.; Pence, N.; Schut, G. J.; Jones, A. K.; Soltis, S. M.; Adams, M. W. W.; Raugei, S.; King, P. W.; Peters, J. W. Tuning Catalytic Bias of Hydrogen Gas Producing Hydrogenases. *J. Am. Chem. Soc.* **2020**, *142* (3), 1227–1235. https://doi.org/10.1021/jacs.9b08756.
(16) Nicolet, Y.; Piras, C.; Legrand, P.; Hatchikian, C. E.; Fontecilla-Camps, J. C. *Desulfovibrio desulfuricans* Iron Hydrogenase: The Structure Shows Unusual Coordination to an Active Site Fe Binuclear Center. *Structure* **1999**, *7* (1), 13–23. https://doi.org/10.1016/S0969-2126(99)80005-7.
(17) Silakov, A.; Wenk, B.; Reijerse, E.; Lubitz, W. ^{14}N HYSCORE Investigation of the H-Cluster of [FeFe] Hydrogenase: Evidence for a Nitrogen in the Dithiol Bridge. *Phys. Chem. Chem. Phys.* **2009**, *11* (31), 6592–6599. https://doi.org/10.1039/b905841a.
(18) Cornish, A. J.; Gärtner, K.; Yang, H.; Peters, J. W.; Hegg, E. L. Mechanism of Proton Transfer in [FeFe]-Hydrogenase from *Clostridium pasteurianum*. *J. Biol. Chem.* **2011**, *286* (44), 38341–38347. https://doi.org/10.1074/jbc.M111.254664.
(19) Morra, S.; Giraudo, A.; Di Nardo, G.; King, P. W.; Gilardi, G.; Valetti, F. Site Saturation Mutagenesis Demonstrates a Central Role for Cysteine 298 as Proton Donor to the Catalytic Site in *Ca*HydA [FeFe]-Hydrogenase. *PLoS ONE* **2012**, *7* (10:e48400), 1–8. https://doi.org/10.1371/journal.pone.0048400.

(20) Winkler, M.; Senger, M.; Duan, J.; Esselborn, J.; Wittkamp, F.; Hofmann, E.; Apfel, U.-P.; Stripp, S. T.; Happe, T. Accumulating the Hydride State in the Catalytic Cycle of [FeFe]-Hydrogenases. *Nat. Commun.* **2017**, *8* (16115), 1–7. https://doi.org/10.1038/ncomms16115.
(21) Puthenkalathil, R. C.; Ensing, B. Fast Proton Transport in FeFe Hydrogenase via a Flexible Channel and a Proton Hole Mechanism. *J. Phys. Chem. B* **2022**, *126* (2), 403–411. https://doi.org/10.1021/acs.jpcb.1c08124.
(22) Lampret, O.; Duan, J.; Hofmann, E.; Winkler, M.; Armstrong, F. A.; Happe, T. The Roles of Long-Range Proton-Coupled Electron Transfer in the Directionality and Efficiency of [FeFe]-Hydrogenases. *Proc. Natl. Acad. Sci. U.S.A.* **2020**, *117* (34), 20520–20529. https://doi.org/10.1073/pnas.2007090117.
(23) Duan, J.; Senger, M.; Esselborn, J.; Engelbrecht, V.; Wittkamp, F.; Apfel, U.-P.; Hofmann, E.; Stripp, S. T.; Happe, T.; Winkler, M. Crystallographic and Spectroscopic Assignment of the Proton Transfer Pathway in [FeFe]-Hydrogenases. *Nat. Commun.* **2018**, *9* (4726), 1–11. https://doi.org/10.1038/s41467-018-07140-x.
(24) Senger, M.; Eichmann, V.; Laun, K.; Duan, J.; Wittkamp, F.; Knör, G.; Apfel, U.-P.; Happe, T.; Winkler, M.; Heberle, J.; Stripp, S. T. How [FeFe]-Hydrogenase Facilitates Bidirectional Proton Transfer. *J. Am. Chem. Soc.* **2019**, *141* (43), 17394–17403. https://doi.org/10.1021/jacs.9b09225.
(25) Chongdar, N.; Birrell, J. A.; Pawlak, K.; Sommer, C.; Reijerse, E. J.; Rüdiger, O.; Lubitz, W.; Ogata, H. Unique Spectroscopic Properties of the H-Cluster in a Putative Sensory [FeFe] Hydrogenase. *J. Am. Chem. Soc.* **2018**, *140* (3), 1057–1068. https://doi.org/10.1021/jacs.7b11287.
(26) Calusinska, M.; Joris, B.; Wilmotte, A. Genetic Diversity and Amplification of Different Clostridial [FeFe] Hydrogenases by Group-Specific Degenerate Primers: Amplification of [FeFe] Hydrogenases. *Lett. Appl. Microbiol.* **2011**, *53* (4), 473–480. https://doi.org/10.1111/j.1472-765X.2011.03135.x.
(27) Bruska, M. K.; Stiebritz, M. T.; Reiher, M. Regioselectivity of H Cluster Oxidation. *J. Am. Chem. Soc.* **2011**, *133* (50), 20588–20603. https://doi.org/10.1021/ja209165r.
(28) Swanson, K. D.; Ratzloff, M. W.; Mulder, D. W.; Artz, J. H.; Ghose, S.; Hoffman, A.; White, S.; Zadvornyy, O. A.; Broderick, J. B.; Bothner, B.; King, P. W.; Peters, J. W. [FeFe]-Hydrogenase Oxygen Inactivation Is Initiated at the H Cluster 2Fe Subcluster. *J. Am. Chem. Soc.* **2015**, *137* (5), 1809–1816. https://doi.org/10.1021/ja510169s.
(29) Esselborn, J.; Kertess, L.; Apfel, U.-P.; Hofmann, E.; Happe, T. Loss of Specific Active-Site Iron Atoms in Oxygen-Exposed [FeFe]-Hydrogenase Determined by Detailed X-Ray Structure Analyses. *J. Am. Chem. Soc.* **2019**, *141* (44), 17721–17728. https://doi.org/10.1021/jacs.9b07808.
(30) Mebs, S.; Kositzki, R.; Duan, J.; Kertess, L.; Senger, M.; Wittkamp, F.; Apfel, U.-P.; Happe, T.; Stripp, S. T.; Winkler, M.; Haumann, M. Hydrogen and Oxygen Trapping at the H-Cluster of [FeFe]-Hydrogenase Revealed by Site-Selective Spectroscopy and QM/MM Calculations. *Biochim. Biophys. Acta Bioenerg.* **2018**, *1859* (1), 28–41. https://doi.org/10.1016/j.bbabio.2017.09.003.
(31) Morra, S.; Arizzi, M.; Valetti, F.; Gilardi, G. Oxygen Stability in the New [FeFe]-Hydrogenase from *Clostridium beijerinckii* SM10 (*Cb*A5H). *Biochem.* **2016**, *55* (42), 5897–5900. https://doi.org/10.1021/acs.biochem.6b00780.
(32) Corrigan, P. S.; Tirsch, J. L.; Silakov, A. Investigation of the Unusual Ability of the [FeFe] Hydrogenase from *Clostridium beijerinckii* to Access an O_2-Protected State. *J. Am. Chem. Soc.* **2020**, *142* (28), 12409–12419. https://doi.org/10.1021/jacs.0c04964.
(33) Pandelia, M.-E.; Ogata, H.; Lubitz, W. Intermediates in the Catalytic Cycle of [NiFe] Hydrogenase: Functional Spectroscopy of the Active Site. *Chem. Eur. J. of Chem. Phys.* **2010**, *11* (6), 1127–1140. https://doi.org/10.1002/cphc.200900950.
(34) Kulka-Peschke, C. J.; Schulz, A.-C.; Lorent, C.; Rippers, Y.; Wahlefeld, S.; Preissler, J.; Schulz, C.; Wiemann, C.; Bernitzky, C. C. M.; Karafoulidi-Retsou, C.; Wrathall, S. L. D.; Procacci, B.; Matsuura, H.; Greetham, G. M.; Teutloff, C.; Lauterbach, L.; Higuchi, Y.; Ishii, M.; Hunt, N. T.; Lenz, O.; Zebger, I.; Horch, M. Reversible Glutamate Coordination to High-Valent Nickel Protects the Active Site of a [NiFe] Hydrogenase from Oxygen. *J. Am. Chem. Soc.* **2022**, *144* (37), 17022–17032. https://doi.org/10.1021/jacs.2c06400.

(35) Ogata, H.; Lubitz, W.; Higuchi, Y. Structure and Function of [NiFe] Hydrogenases. *J. Biochem.* **2016**, *160* (5), 251–258. https://doi.org/10.1093/jb/mvw048.
(36) Winkler, M.; Duan, J.; Rutz, A.; Felbek, C.; Scholtysek, L.; Lampret, O.; Jaenecke, J.; Apfel, U.-P.; Gilardi, G.; Valetti, F.; Fourmond, V.; Hofmann, E.; Léger, C.; Happe, T. A Safety Cap Protects Hydrogenase from Oxygen Attack. *Nat. Commun.* **2021**, *12* (756), 1–10. https://doi.org/10.1038/s41467-020-20861-2.
(37) Rodríguez-Maciá, P.; Reijerse, E. J.; van Gastel, M.; DeBeer, S.; Lubitz, W.; Rüdiger, O.; Birrell, J. A. Sulfide Protects [FeFe] Hydrogenases From O_2. *J. Am. Chem. Soc.* **2018**, *140* (30), 9346–9350. https://doi.org/10.1021/jacs.8b04339.
(38) Rutz, A.; Das, C. K.; Fasano, A.; Jaenecke, J.; Yadav, S.; Apfel, U.-P.; Engelbrecht, V.; Fourmond, V.; Léger, C.; Schäfer, L. V.; Happe, T. Increasing the O_2 Resistance of the [FeFe]-Hydrogenase *Cb*A5H through Enhanced Protein Flexibility. *ACS Catal.* **2023**, *13* (2), 856–865. https://doi.org/10.1021/acscatal.2c04031.
(39) Rodríguez-Maciá, P.; Pawlak, K.; Rüdiger, O.; Reijerse, E. J.; Lubitz, W.; Birrell, J. A. Intercluster Redox Coupling Influences Protonation at the H-Cluster in [FeFe] Hydrogenases. *J. Am. Chem. Soc.* **2017**, *139* (42), 15122–15134. https://doi.org/10.1021/jacs.7b08193.
(40) Senger, M.; Mebs, S.; Duan, J.; Shulenina, O.; Laun, K.; Kertess, L.; Wittkamp, F.; Apfel, U.-P.; Happe, T.; Winkler, M.; Haumann, M.; Stripp, S. T. Protonation/Reduction Dynamics at the [4Fe–4S] Cluster of the Hydrogen-Forming Cofactor in [FeFe]-Hydrogenases. *Phys. Chem. Chem. Phys.* **2018**, *20* (5), 3128–3140. https://doi.org/10.1039/C7CP04757F.
(41) Senger, M.; Duan, J.; Pavliuk, M. V.; Apfel, U.-P.; Haumann, M.; Stripp, S. T. Trapping an Oxidized and Protonated Intermediate of the [FeFe]-Hydrogenase Cofactor under Mildly Reducing Conditions. *Inorg. Chem.* **2022**, *61* (26), 10036–10042. https://doi.org/10.1021/acs.inorgchem.2c00954.
(42) Martini, M. A.; Rüdiger, O.; Breuer, N.; Nöring, B.; DeBeer, S.; Rodríguez-Maciá, P.; Birrell, J. A. The Nonphysiological Reductant Sodium Dithionite and [FeFe] Hydrogenase: Influence on the Enzyme Mechanism. *J. Am. Chem. Soc.* **2021**, *143* (43), 18159–18171. https://doi.org/10.1021/jacs.1c07322.
(43) Salis, A.; Monduzzi, M. Not Only PH. Specific Buffer Effects in Biological Systems. *J. Colloid Interface Sci.* **2016**, *23*, 1–9. https://doi.org/10.1016/j.cocis.2016.04.004.
(44) Loreto, S.; Cuypers, B.; Brokken, J.; Van Doorslaer, S.; De Wael, K.; Meynen, V. The Effect of the Buffer Solution on the Adsorption and Stability of Horse Heart Myoglobin on Commercial Mesoporous Titanium Dioxide: A Matter of the Right Choice. *Phys. Chem. Chem. Phys.* **2017**, *19* (21), 13503–13514. https://doi.org/10.1039/C6CP08585G.
(45) Brudar, S.; Hribar-Lee, B. Effect of Buffer on Protein Stability in Aqueous Solutions: A Simple Protein Aggregation Model. *J. Phys. Chem. B* **2021**, *125* (10), 2504–2512. https://doi.org/10.1021/acs.jpcb.0c10339.
(46) Taha, M.; Lee, M.-J. Interactions of TRIS [Tris(Hydroxymethyl)Aminomethane] and Related Buffers with Peptide Backbone: Thermodynamic Characterization. *Phys. Chem. Chem. Phys.* **2010**, *12* (39), 12840–12850. https://doi.org/10.1039/c0cp00253d.
(47) Silakov, A.; Reijerse, E. J.; Albracht, S. P. J.; Hatchikian, E. C.; Lubitz, W. The Electronic Structure of the H-Cluster in the [FeFe]-Hydrogenase from *Desulfovibrio desulfuricans* : A Q-Band ^{57}Fe-ENDOR and HYSCORE Study. *J. Am. Chem. Soc.* **2007**, *129* (37), 11447–11458. https://doi.org/10.1021/ja072592s.
(48) Myers, W. K.; Stich, T. A.; Suess, D. L. M.; Kuchenreuther, J. M.; Swartz, J. R.; Britt, R. D. The Cyanide Ligands of [FeFe] Hydrogenase: Pulse EPR Studies of ^{13}C and ^{15}N-Labeled H-Cluster. *J. Am. Chem. Soc.* **2014**, *136* (35), 12237–12240. https://doi.org/10.1021/ja507046w.
(49) Gilbert-Wilson, R.; Siebel, J. F.; Adamska-Venkatesh, A.; Pham, C. C.; Reijerse, E.; Wang, H.; Cramer, S. P.; Lubitz, W.; Rauchfuss, T. B. Spectroscopic Investigations of [FeFe] Hydrogenase Maturated with [$^{57}Fe_2(Adt)(CN)_2(CO)_4]^{2-}$. *J. Am. Chem. Soc.* **2015**, *137* (28), 8998–9005. https://doi.org/10.1021/jacs.5b03270.

(50) Rao, G.; Britt, R. D. Electronic Structure of Two Catalytic States of the [FeFe] Hydrogenase H-Cluster As Probed by Pulse Electron Paramagnetic Resonance Spectroscopy. *Inorg. Chem.* **2018**, *57* (17), 10935–10944. https://doi.org/10.1021/acs.inorgchem.8b01557.
(51) del Barrio, M.; Sensi, M.; Fradale, L.; Bruschi, M.; Greco, C.; de Gioia, L.; Bertini, L.; Fourmond, V.; Léger, C. Interaction of the H-Cluster of FeFe Hydrogenase with Halides. *J. Am. Chem. Soc.* **2018**, *140* (16), 5485–5492. https://doi.org/10.1021/jacs.8b01414.
(52) Senger, M.; Mebs, S.; Duan, J.; Wittkamp, F.; Apfel, U.-P.; Heberle, J.; Haumann, M.; Stripp, S. T. Stepwise Isotope Editing of [FeFe]-Hydrogenases Exposes Cofactor Dynamics. *Proc. Natl. Acad. Sci. U.S.A.* **2016**, *113* (30), 8454–8459. https://doi.org/10.1073/pnas.1606178113.
(53) Fourmond, V.; Greco, C.; Sybirna, K.; Baffert, C.; Wang, P.-H.; Ezanno, P.; Montefiori, M.; Bruschi, M.; Meynial-Salles, I.; Soucaille, P.; Blumberger, J.; Bottin, H.; De Gioia, L.; Léger, C. The Oxidative Inactivation of FeFe Hydrogenase Reveals the Flexibility of the H-Cluster. *Nature Chem.* **2014**, *6* (4), 336–342. https://doi.org/10.1038/nchem.1892.
(54) Heghmanns, M.; Rutz, A.; Kutin, Y.; Engelbrecht, V.; Winkler, M.; Happe, T.; Kasanmascheff, M. The Oxygen-Resistant [FeFe]-Hydrogenase *Cb*A5H Harbors an Unknown Radical Signal. *Chem. Sci.* **2022**, *13* (24), 7289–7294. https://doi.org/10.1039/D2SC00385F.
(55) Noodleman, L.; Peng, C. Y.; Case, D. A.; Mouesca, J.-M. Orbital Interactions, Electron Delocalization and Spin Coupling in Iron-Sulfur Clusters. *Coord. Chem. Rev.* **1995**, *144*, 199–244. https://doi.org/10.1016/0010-8545(95)07011-L.
(56) Mouesca, J.-M.; Chen, J. L.; Noodleman, L.; Bashford, D.; Case, D. A. Density Functional/Poisson-Boltzmann Calculations of Redox Potentials for Iron-Sulfur Clusters. *J. Am. Chem. Soc.* **1994**, *116* (26), 11898–11914. https://doi.org/10.1021/ja00105a033.
(57) Silakov, A.; Reijerse, E. J.; Lubitz, W. Unraveling the Electronic Properties of the Photoinduced States of the H-Cluster in the [FeFe] Hydrogenase from *D. desulfuricans*. *Eur. J. Inorg. Chem.* **2011**, *2011* (7), 1056–1066. https://doi.org/10.1002/ejic.201001080.
(58) Bominaar, E. L.; Hu, Z.; Muenck, E.; Girerd, J.-J.; Borshch, S. A. Double Exchange and Vibronic Coupling in Mixed-Valence Systems. Electronic Structure of Exchange-Coupled Siroheme-[Fe4S4]$^{2+}$ Chromophore in Oxidized *E. Coli* Sulfite Reductase. *J. Am. Chem. Soc.* **1995**, *117* (26), 6976–6989. https://doi.org/10.1021/ja00131a021.
(59) Belinsky, M. I. Induced Paramagnetism and Hyperfine Interactions in the {[Fe_4S_4]-Fe} Active Site of *Escherichia Coli* Sulfite Reductase. *Chem. Phys. Lett.* **1996**, *250* (3), 320–327. https://doi.org/10.1016/0009-2614(95)01456-X.
(60) Popescu, C. V.; Münck, E. Electronic Structure of the H Cluster in [Fe]-Hydrogenases. *J. Am. Chem. Soc.* **1999**, *121* (34), 7877–7884. https://doi.org/10.1021/ja991243y.
(61) Xia, J.; Hu, Z.; Popescu, C. V.; Lindahl, P. A.; Münck, E. Mössbauer and EPR Study of the Ni-Activated R-Subunit of Carbon Monoxide Dehydrogenase from *Clostridium Thermoaceticum*. *J. Am. Chem. Soc.* **1997**, *119* (35), 8301–8312.
(62) Le Pape, L.; Lamotte, B.; Mouesca, J.-M.; Rius, G. Paramagnetic States of Four Iron−Four Sulfur Clusters. 1. EPR Single-Crystal Study of 3+ and 1+ Clusters of an Asymmetrical Model Compound and General Model for the Interpretation of the g-Tensors of These Two Redox States. *J. Am. Chem. Soc.* **1997**, *119* (41), 9757–9770. https://doi.org/10.1021/ja963349o.
(63) Pandelia, M.-E.; Lanz, N. D.; Booker, S. J.; Krebs, C. Mössbauer Spectroscopy of Fe/S Proteins. *Biochim. Biophys. Acta Mol. Cell. Res.* **2015**, *1853* (6), 1395–1405. https://doi.org/10.1016/j.bbamcr.2014.12.005.
(64) Beinert, H.; Holm, R. H.; Münck, E. Iron-Sulfur Clusters: Nature's Modular, Multipurpose Structures. *Science* **1997**, *277* (5326), 653–659. https://doi.org/10.1126/science.277.5326.653.
(65) Yoo, S. J.; Meyer, J.; Achim, C.; Peterson, J.; Hendrich, M. P.; Münck, E. Mössbauer, EPR, and MCD Studies of the C9S and C42S Variants of *Clostridium pasteurianum* Rubredoxin and MCD Studies of the Wild-Type Protein. *J. Biol. Inorg. Chem.* **2000**, *5* (4), 475–487. https://doi.org/10.1007/s007750050008.

(66) Zadrozny, J. M.; Greer, S. M.; Hill, S.; Freedman, D. E. A Flexible Iron(II) Complex in Which Zero-Field Splitting Is Resistant to Structural Variation. *Chem. Sci.* **2016**, *7* (1), 416–423. https://doi.org/10.1039/C5SC02477C.
(67) Mouesca, J.-M.; Rius, G.; Lamotte, B. Single-Crystal Proton ENDOR Studies of the $[Fe4S4]^{3+}$ Cluster: Determination of the Spin Population Distribution and Proposal of a Model to Interpret the ^{1}H NMR Paramagnetic Shifts in High-Potential Ferredoxins. *J. Am. Chem. Soc.* **1993**, *115* (11), 4714–4731. https://doi.org/10.1021/ja00064a036.
(68) Kolling, D. R. J.; Samoilova, R. I.; Shubin, A. A.; Crofts, A. R.; Dikanov, S. A. Proton Environment of Reduced Rieske Iron−Sulfur Cluster Probed by Two-Dimensional ESEEM Spectroscopy. *J. Phys. Chem. A* **2009**, *113* (4), 653–667. https://doi.org/10.1021/jp806789x.
(69) Le Pape, L.; Lamotte, B.; Mouesca, J.-M.; Rius, G. Paramagnetic States of Four Iron−Four Sulfur Clusters. 2. Proton ENDOR Study of a 1+ State in an Asymmetrical Cluster. *J. Am. Chem. Soc.* **1997**, *119* (41), 9771–9781. https://doi.org/10.1021/ja963350n.
(70) Sidabras, J. W.; Duan, J.; Winkler, M.; Happe, T.; Hussein, R.; Zouni, A.; Suter, D.; Schnegg, A.; Lubitz, W.; Reijerse, E. J. Extending Electron Paramagnetic Resonance to Nanoliter Volume Protein Single Crystals Using a Self-Resonant Microhelix. *Sci. Adv.* **2019**, *5* (eaay1394), 1–11. https://doi.org/10.1126/sciadv.aay1394.

TABLE OF CONTENTS GRAPHIC